

Article

Study on Propellers Distribution and Flow Field in the Oxidation Ditch Based on Two-Phase CFD Model

Yuquan Zhang ¹, Chengyi Li ^{2,*}, Yanhe Xu ³, Qinghong Tang ², Yuan Zheng ¹, Huiwen Liu ¹ and E. Fernandez-Rodriguez ⁴

¹ College of Energy and Electrical Engineering, Hohai University, Nanjing 210098, China;

zhangyq@hhu.edu.cn (Y.Z.); zhengyuan@hhu.edu.cn (Y.Z.); huiwen_liu@hhu.edu.cn (H.L.)

² College of Water Conservancy and Hydropower Engineering, Hohai University, Nanjing 210098, China; tangqhr@hhu.edu.cn

³ School of Hydropower and Information Engineering, Huazhong University of Science and Technology, Wuhan 430074, China; yh_xu@hust.edu.cn

⁴ Technological Institute of Merida, Technological Avenue, Merida 97118, Mexico; fratellosole22@hotmail.com

* Correspondence: vghead@163.com; Tel.: +86-159-5050-6256

Received: 15 October 2019; Accepted: 25 November 2019; Published: 27 November 2019



Abstract: The oxidation ditch (OD) plays an important role in wastewater treatment plants. With increasing demand and production costs, the energy consumption and sludge deposition occurring in the OD must be diminished to enhance its development. In this paper, a two-phase computational fluid dynamics (CFD) model of water and activated sludge examined the flow field characteristics of an OD, consisting of two side-by-side propellers. The system was studied under five configurations, where the spacing between the propellers was set equal to -0.2 , -0.1 , 0 , 0.1 , 0.2 times the length of the OD. The viscosity and settling rate of activated sludge was imported in the numerical simulation through a user defined function (UDF). The optimal scheme of the propeller's power consumption, velocity distribution, and sludge concentration distribution was obtained. The result shows that sludge concentrations are linked with dead zone velocity but not necessarily with low velocities. Experiments confirmed the validity of the velocity flow field simulated by the two-phase CFD model. Overall, these findings form the basis for the propellers distribution optimization and allow a deeper insight into the flow field of OD systems.

Keywords: oxidation ditch; two-phase CFD; flow field; sludge concentration; submerged propeller

1. Introduction

To deal with the rapid increase in wastewater, lots of treatment plants have been installed to clean and reuse the water in industrial processes [1]. Currently, about 32.1% of the Chinese wastewater treatment plants employ the use of the oxidation ditch (OD) [2]. The OD, also known as the continuous loop reactor, is a cyclic aeration system used to remove the organic matter from residual flows. Key aspects of ODs include their simplicity, low sludge production, and confidence in the market, including operation and maintenance processes [3]. Therefore, they are one of the most widely used methods for activated sludge biological treatment [4]. Despite the existing research recognizes the critical role played by OD in the treatment plant's production effectiveness and economics, old and inefficient technology still prevails in many OD systems; thus, studies suggest their modernization will enhance the flow field and reduce costs and environmental impact [5–8].

Since the primary concern of an OD relies on the hydrodynamic characteristics of the operating flow, its predictions through engineering tools, such as computational fluid dynamics (CFD), become important and are a concern in the plant design and economics [9–12]. Traditionally, studies of

OD systems have treated the water and suspended solids as a single phase to determine the flow patterns and OD optimal configurations. Luo et al. [13] simulated the flow field in a small OD by the Reynolds-Averaged Navier-Stokes (RANS) equation. The flow pattern was analyzed in detail, and both trials and simulations were found to be similar. Zhang et al. [3] experimentally validated a CFD model to optimize the energy consumption and flow field. The least power density and requirement of the flow pattern were obtained and validated against physical tests. Yang et al. [14] used a moving wall method to show the suitability of a more complex, 3D single-phase CFD method, whilst Wu et al. [15] conducted a numerical simulation based on a standard $k - \epsilon$ turbulence model to optimize the installation of submerged propellers in OD. According to results, the sludge deposit due to low velocity was avoided in the optimal arrangement of the propellers. In particular, both the influence of position and energy consumed by single and multiple impellers is a continuing concern within OD systems.

In the investigation conducted by Hartley [16], the author described the design and implementation of a process for settling the sludge deposits. By using a single-phase model, Gancarski [17] studied the settling of sludge on the basis of tracking the particles. However, the concept of sludge concentration of suspended solids was not an important aspect in the simulations. Likewise, by treating the sludge as a single-phase scalar, Brannock [18] investigated the wastewater behavior in the vessel. Importantly, for the above studies, the setting of the minimum velocity [19–23] in the single-phase model and the neglect of the other phases have been subject to debate within the research community. The single-phase approach, although being practical and computationally effective, it suffers from simulating high suspended-solid concentrations in ODs.

Therefore, it is essential to include the liquid–solid phase to investigate the sludge settling and flow field in the simulation. To date, only a few multi-phase works have investigated the influence of propeller positions on the hydrodynamic characteristics of the OD. In the studies of Yang et al. [1], a two-phase CFD model was put forward to optimize the flow field and dissolved oxygen concentration in the OD. The model was able to predict the oxygen mass transfer features and flow patterns equipped with submerged impellers, although it was limited to treat water and suspended solids as a single phase leading to the disparity between results and trials. To gain a fuller understanding, Xie et al. [2] proposed a modified two-phase CFD model to investigate the distribution of suspended solids, thus showing that the model can help optimization of design and operation of the OD. Fan et al. [24] focused on the hydrodynamics of the turbulent two-phase (liquid–solid) flow in an OD by simulating the flow field with surface aerators. The results of liquid velocity and volume variation formed the basis for the optimization of OD. In the study of Climent et al. [4], a two-phase CFD model was investigated to improve the hydraulic characteristics in the OD, which provides a further understanding of the interaction between liquid behavior and phase motion. However, there is a limited understanding of the mechanism of the flow field characteristics influenced by the propeller's arrangement and sludge concentration.

In view of the above, the aim of this paper is to study, through a two-phase CFD model, the characteristics of flow and sludge distribution of a full-scale OD. In the model, the viscosity and settling rate of the activated sludge is defined in terms of user defined function (UDF), and the speed of the propellers is selected based on the energy requirement of the OD. An optimal scheme is then determined on the basis of flow field characteristics by changing the position of the propellers. Finally, this arrangement is further analyzed and compared with the experimental data.

2. Materials and Methods

2.1. Parameters of Experiments

A conventional OD of the sewage treatment plant was used in the investigation, as shown in Figure 1. The length (L) of the OD is 48.6 m, the width (W) is 12.3 m, and the depth (h) is 6.5 m. The height of the liquid level is 6 m above the bottom of the ditch, and that of the propeller axle is



Figure 4. LJ20A-type convenient tachymeter.

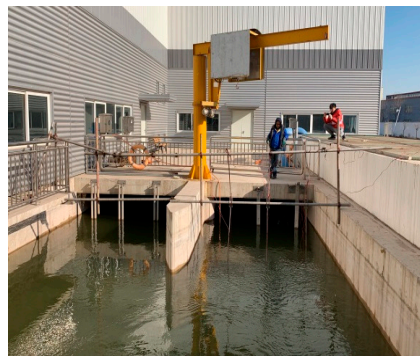


Figure 5. The tachymeters installed on the bracket.

2.2. Numerical Simulation

2.2.1. Governing Equations

The flows in the OD are by nature highly turbulent, and therefore, the most common, less intensive resource tool to model them is through the solution of the RANS equations [3,26–28]. These equations apply the Reynolds decomposition in the velocity and pressure [29], as follows:

$$\text{Continuity : } \frac{\partial \bar{u}_i}{\partial x_i} = 0, \quad (1)$$

$$\text{Momentum: } \rho \frac{\partial \bar{u}_i}{\partial t} + \rho \frac{\partial (\bar{u}_i \bar{u}_j)}{\partial x_j} = \rho \bar{f}_i + \frac{\partial}{\partial x_j} \left(-\bar{p} \delta_{ij} + 2\mu \bar{S}_{ij} - \rho \overline{u'_i u'_j} \right), \quad (2)$$

where u_i is velocity, x_i is the spatial co-ordinate, p is the pressure, ρ is the fluid density, μ is the dynamic viscosity, \bar{f}_i the time mean external force tensor, and $\bar{S}_{ij} = 0.5(\partial \bar{u}_i / \partial x_j + \partial \bar{u}_j / \partial x_i)$ is the mean rate of the strain tensor. The Dirac function is $\delta_{ij} = 1$ for $i = j$ and zero otherwise. To closure the RANS equations, the Reynolds stresses $\overline{u'_i u'_j}$ requires the use of a turbulence model. The $k - \varepsilon$ turbulence model [3] is adopted to account for the swirl and secondary flow phenomenon in the curve of the OD.

The mixture model adopts a two-phase flow representation. The first item is the water-liquid coming from the material library, and the second one is the activated sludge, in this paper. The density of clean water is 998.2 kg/m^3 , and the viscosity is $0.001003 \text{ Pa}\cdot\text{s}$. The activated sludge has a density of 1050 kg/m^3 , and its viscosity is influenced by the temperature and concentration. The liquid temperature used in this paper was $25 \text{ }^\circ\text{C}$, which is 298.15 K . According to [30,31], the sludge viscosity is most affected by the sludge concentration, while the effect of temperature is comparatively smaller.

In the condition of sludge concentration less than 60 g/L and liquid temperature ranging from 12 °C to 32 °C, the equation of sludge viscosity could be obtained by the index model. The expression is:

$$\mu_{sv} = 0.63 \exp\left(\frac{120}{T} + 0.078MLSS\right), \quad (3)$$

where μ_{sv} is sludge viscosity, 10^{-3} Pa·s, T is absolute temperature, K, $MLSS$ represents the mixed liquor suspended solids, g/L.

The sedimentation rate of sludge in clean water is obtained according to the double-index sludge sedimentation model [2]. The given procedure initially consists of measuring the sedimentation rate of sludge under different concentrations. Subsequently, these are fitted into formulations to obtain the following coefficients:

$$V_s = 0.004 \times (e^{-0.46x} - e^{-1.86x}), \quad (4)$$

where V_s is sludge sedimentation rate, m/s; x indicates sludge concentration, g/L.

Equations (3) and (4) were applied by UDF and introduced into ANSYS Fluent [3]. The viscosity and settling rate of the activated sludge were defined, where the particle diameter of sludge was 0.4 mm. Prior to the two-phase flow calculation, the result of the single-phase flow was firstly introduced into the ANSYS Fluent as the initial condition of the full flow field.

2.2.2. Geometry and Mesh Grid

The three-dimensional model of the OD was established by using the software of Unigraphics NX (UG). The blade has a radius of 1.25 m, a root thickness of 0.04 m, and a tip thickness of 0.036 m. The hub radius is 0.1 m. A rotating region with a radius of 1.4 m and a height of 0.89 m was created for each impeller. According to the concept of energy balance, the fluid in this region obtains and transfers energy to the surrounding liquids. The whole area of the OD was divided into the OD flow channel and the submerged propeller region.

Tetrahedral meshes were selected for the control of flow direction, distribution, and the orthogonality of the boundary layer direction. The small parts, such as the blade edge, were locally encrypted, and the number of the overall meshes was set as 2.5 million, 3.9 million, 4.3 million, and 5.1 million. Table 1 illustrates the variation of the evaluation index caused by the mesh density.

Table 1. Variation of the evaluation index.

Mesh Density	Number of Elements (million)	Consumed Power	Consumed Power (kW)
Coarse	2.5	5.2%	3.717
Medium-coarse	3.9	1.4%	3.866
Medium	4.3	0.3%	3.910
Fine	5.1	–	3.921

As clearly seen in the table, as the number of grids increases, the power consumed by the submerged propeller gradually decreases. When the mesh number reaches 4.3 million, the trend of power consumption reduction is no longer obvious, but using a larger number of elements translates into more computer resources. Therefore, a medium mesh with 4.3 million elements is used, and the mesh of the OD is as shown in Figure 6.

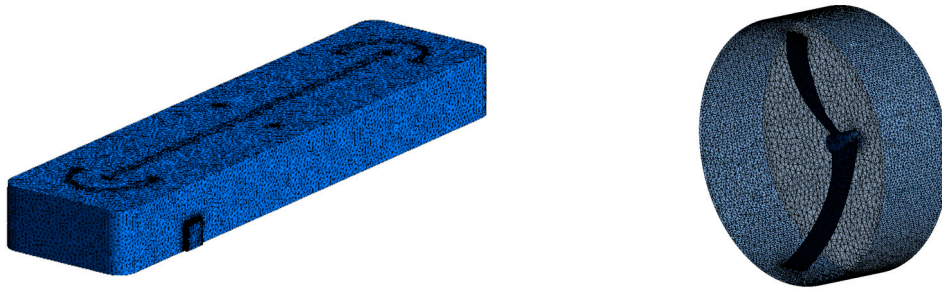


Figure 6. Mesh of the oxidation ditch and rotor.

2.2.3. Boundary Conditions

The flow rate boundary condition was assigned at the inlet with the value of 1331.11 kg/s, while the zero pressure was set at the outlet. The symmetry boundary condition was adopted at the water surface. The no-slip boundary conditions were applied in the bottom surface, side wall, bracket, and curved wall. The wall surface was cement, and the surface roughness was set as 0.5 mm based on the test condition and our previous work of simulation [3]. The finite volume method was applied to discretize the governing equations. The second-order central difference scheme was adopted in the diffusion term, and the second-order upwind style was used in the convection term. The SIMPLE algorithm was used in the coupling process of speed and pressure. For the unsteady simulation, the blades rotated one degree per time step.

3. Results and Discussion

3.1. Determination of the Power Consumption

The power consumption of the submerged propeller was obtained after determining the liquid medium and type of the OD, in accordance to the methodology provided by the LJM company in Denmark [1,32]. This approach includes the energy balance of the oxidation ditch, and it is divided into three parts:

(1) Requirement for pushing 1-kg liquid,

$$H_f = \frac{(\Sigma\xi + \lambda \frac{U_w L}{F}) U^2}{2} = 0.43 \text{ J/kg}, \quad (5)$$

where $\Sigma\xi$ is the overall local resistance factor; for the 90° circular angle, $\xi = 1$, and for the 90° right angle, $\xi = 1.53$. Since six circular-angled corners exist, thus $\Sigma\xi = 6$. F denotes the discharge area; $\lambda = 0.03$, the frictional resistant coefficient; L , the length of the OD; U_w , the wetted perimeter, and U , the flow velocity.

(2) Losses,

$$W_r = H_f Q_p = 4.64 \text{ kW}, \quad (6)$$

where Q_p is the discharge through the water section of the OD.

(3) And net power,

$$W_R = \frac{W_r}{\eta} = 7.73 \text{ kW}, \quad (7)$$

where η is the efficiency of the propeller; 60% here.

Since two propellers are employed in the study, the minimum power is $W_R/2 = 3.86 \text{ kW}$, thus a rated power of $W_R = 4 \text{ kW}$ is set to ensure a correct operation.

3.2. Distribution of the Propellers

The inlet sludge concentration was set as 3.5 g/L, and the rotating speed of the propeller was 81 r/min. The distribution of the propellers was controlled by changing the longitudinal distance (ΔL) between the two propellers, assuming ($\Delta L < 10$ m for a proper ditch operation [3,15]). Five schemes were studied: $-0.2L$ (a), $-0.1L$ (b), 0 (c), $0.1L$ (d), $0.2L$ (e), as shown in Figure 7.

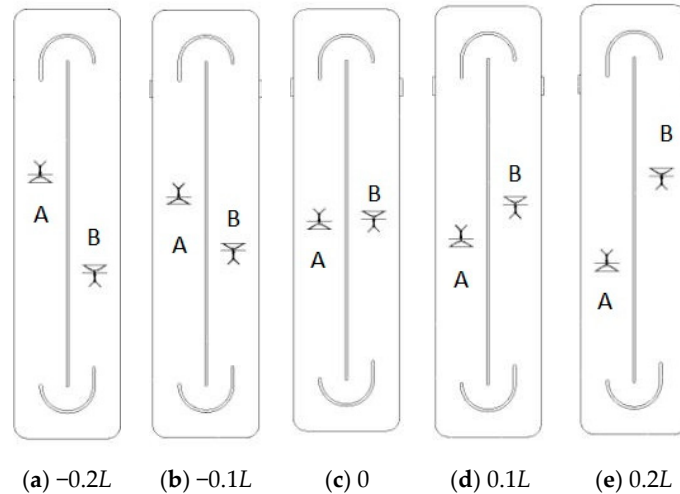


Figure 7. Layout diagram of propeller when $\Delta L = -0.2L \sim 0.2L$.

3.2.1. Velocity Distribution near the Bottom

Since the sludge deposition is most likely to occur when the flow velocity near the bottom of the OD is too low [33]. A horizontal section of 0.3 m from the bottom of the OD was intercepted, and the velocity contour is shown in Figure 8. Clearly, the flow passing the propeller augmented in velocity, forming a high-speed area in the downstream region. Comparing the velocity distribution of the five schemes, it shows that the scheme (b) has the largest high-speed area with a velocity over 0.7 m/s. A low-speed area is basically located below the inlet and around the curved wall, with velocities less than 0.1 m/s. The given trend is more apparent in schemes (c) and (d) rather than in (a) and (b).

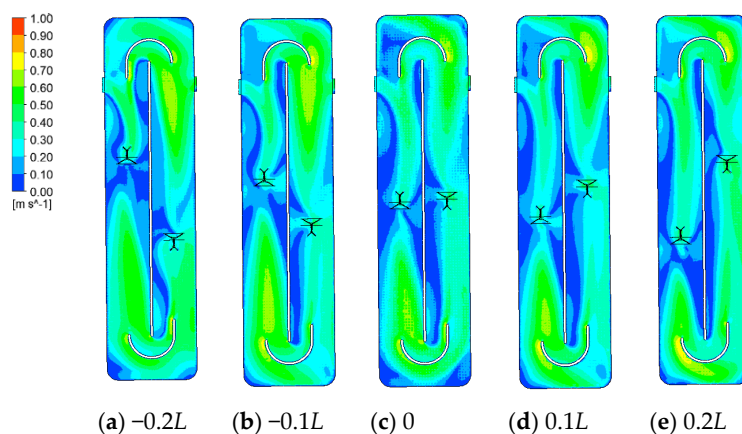


Figure 8. Velocity contour near the bottom of the OD.

In order to quantify and analyze the pros and cons of each scheme, the dead zone rate of different schemes was calculated using a histogram chart of velocities less than 0.1, 0.15, and 0.2 m/s, as shown in Figure 9. In the present report, the term dead zone rate refers to regions with velocities falling below the criterion for significance in the flow field characteristics.

From the data in Figure 9, schemes (a) and (b) contain lower dead zones rates than the remaining cases since propellers were closer to the inlet flow. The distances of the propeller A from the inlet ranged from 11.94 to 14.37 m in schemes (a) and (b). In addition, the propellers farther away from the curved wall produced better performance than other schemes, due to lesser losses produced by flow hitting the wall. A large velocity reduction near the intermediate curved wall is formed in all schemes but (a) and (b) as a result of the centrifugal force in the turn.

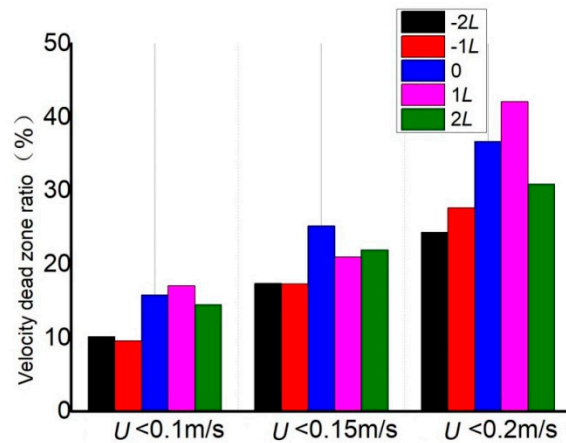


Figure 9. Dead zone rate of different schemes.

3.2.2. Sludge Concentration Distribution near the Bottom

Because the sludge concentration of the ditch is defined in terms of the phase volume fraction of the sludge, contour results near the bottom were obtained, as shown in Figure 10. As observed, the areas of sludge deposition in schemes (a) and (b) are small and mainly located at the two ends of the intermediate curved wall. Remarkably, schemes (c), (d), and (e) develop as well sludge deposition beneath the inlet and behind section of propeller B. Comparing Figure 8 with Figure 9 shows that most of the sludge deposition occurs at the velocity dead zone; hence, this may be used as a parameter to measure the sludge deposition [34].

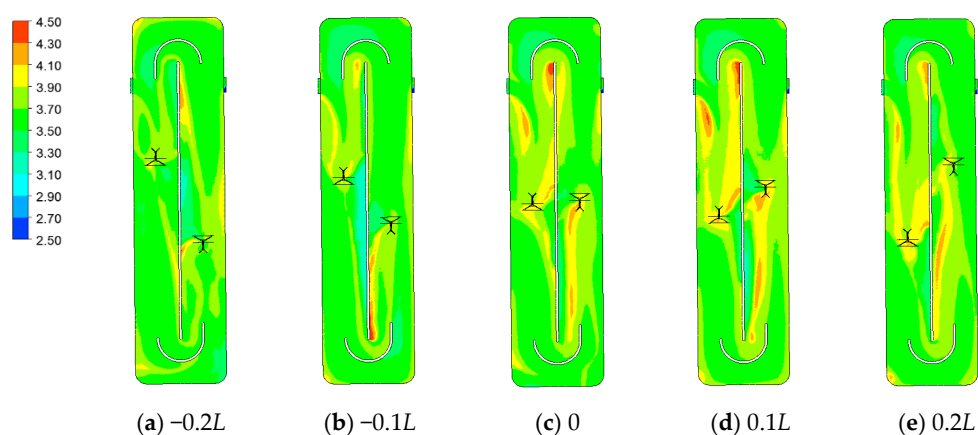


Figure 10. Sludge concentration contour near the bottom of the oxidation ditch.

3.2.3. Sludge Distribution in the Oxidation Ditch

Plane sections at intervals of 0.3 m were set along the water depth direction to calculate the overall sludge concentration, as shown in Figure 11. In the five schemes, the sludge distribution in the oxidation ditch increases gradually from top to bottom, as a consequence of the given settling

rate of sludge and the pushing effect of the propellers. In general, the larger the propeller's push, the larger the uniform sludge distribution along the water depth direction. To quantify the uniformity of sludge distribution, the depth sections influenced by the propellers (0.9–5.1 m) were normalized with the extreme value of sludge concentration variation. For schemes (b), (d), and (e), the extreme value of the sludge concentration per section is relatively small, and the sludge distribution is uniform. Scheme (a) provides the largest extreme value of the sludge concentration, and the rate of change of sludge concentration depths is more pronounced above 2 m. Meanwhile, the sludge distribution is not uniform, thus reducing the treatment effect of the activated sludge on the biochemical and chemical oxygen demand in the sewage. The evidence from this analysis suggests scheme (b) has a more uniform flow velocity and sludge distribution near the bottom of the OD than the other cases, but the dead zone rate and overall sludge concentration of the passage is smaller.

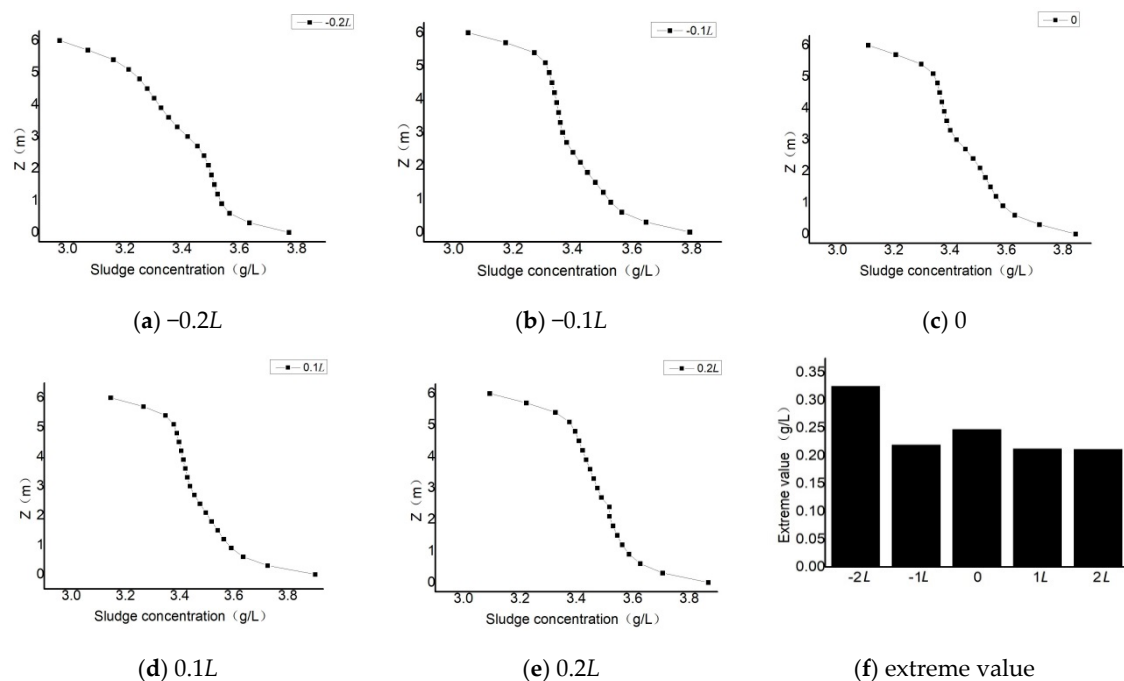


Figure 11. Sludge distribution by different schemes.

3.3. Analysis of Flow Field Characteristics

3.3.1. Analysis of Sludge Concentration and Average Flow Velocity

To examine the links between the scheme (b) and the flow behavior, the variation of the average velocity and the sludge concentration were calculated using the 12 plane sections. As shown in Figure 1, the locations of the sections in the ditch are as follows: section 1, below the inlet of water flow; sections 2–4, running upstream of propeller A; sections 5 and 11, at the curve of wall; sections 7–9, at the second straight; section 10, at the outlet; section 12, at the second curved wall.

The results, as presented in Figure 12, show a scatter trend of the average velocity and sludge concentration at each section. The most surprising aspect of the data was the dissociation of high velocity areas with high sludge concentrations. These differences can be explained in part by the proximity of the section with interferences in the flow. For example, the sections (1, 7–9) close to the propeller have a high velocity, a scatter flow pattern, and low sludge concentration. However, section 1 is located below the inlet of water flow, and its flow pattern is disordered. The increased sludge concentration at the bottom of the inlet side accords with findings of Section 3.2. The curved wall (section 6) augmented these two parameters, as a result of the flow direction. At the propeller's wake, the average velocity and sludge concentration decreased in sections 2–4. Through the strong

guidance of the curved wall, the flow increased in speed, and thus, the sludge concentration was low (sections 5 and 11). The outlet changed the flow direction, resulting in the dead zone flow (section 9); thus, the sludge concentration was high. At the back of the outlet (section 10), since water and sludge flow out from the system, the average flow velocity and the sludge concentration were small. Because the incoming flow impedes the movement of water at the second curved wall, the average velocity was small in section 12.

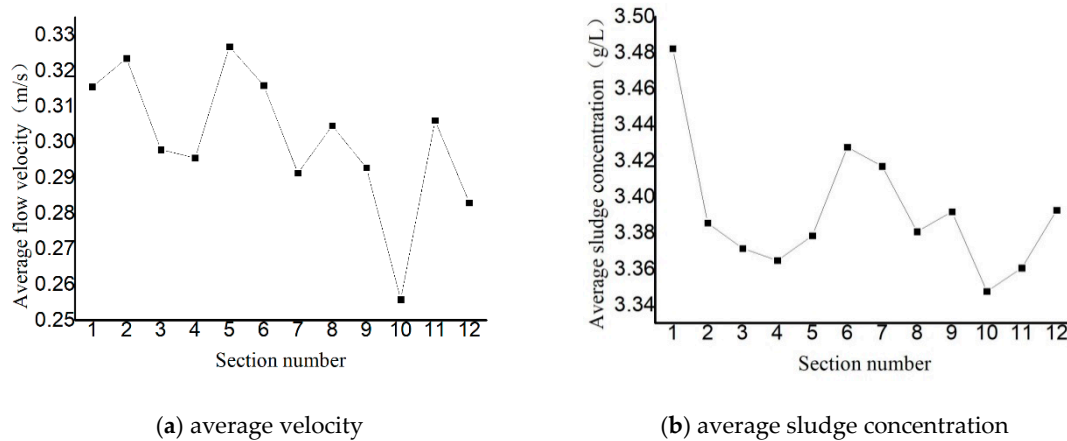


Figure 12. Average velocity and the sludge concentration at 12 plane sections.

3.3.2. Velocity Distribution in Each Section

To develop a deeper understanding of relationships between velocity and locations, the characteristics of the flow field in scheme (b) were analyzed, both experimentally and numerically. This is illustrated in Figure 13 by using six sections (1–6).

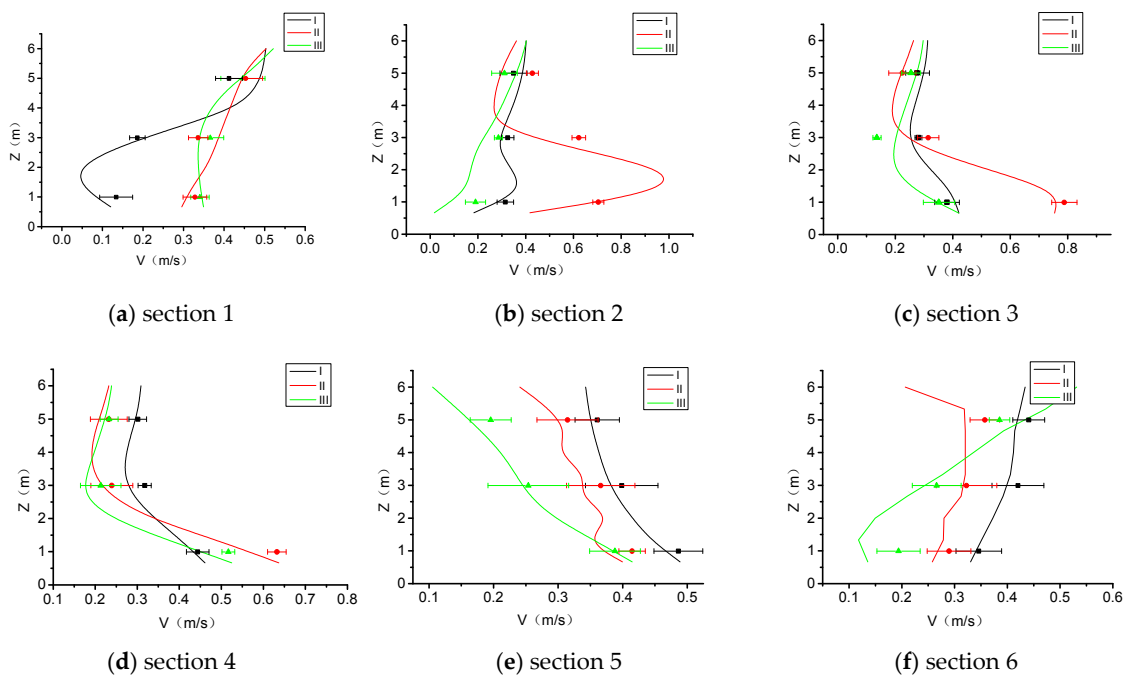


Figure 13. Distribution of flow velocity in each section, simulations (lines) against experiments (markers).

As shown in Figure 13, the experiments have a good consistency with the simulation data. In Figure 12a, propeller A affects little the inlet flow; thus, the flow velocity is stable. However, due to the influence of vertical inlet flow, a vortex is generated near the wall, resulting in a lower velocity near the bottom of measuring points, which is the dark blue area below the inlet in Figure 8, and therefore, the deposition of sludge occurs. Because the pushing effect of the propeller is concentrated in front of the wheel, which is the lower middle of the section, the flow at this point attains the highest speed, up to 1 m/s. The bottom of both sides is not affected by the flow significantly, so the flow velocity is relatively low.

To better understand the propeller's influence on the flow, predictions of velocity vectors are made for sections 3 and 5 (Figure 14). It could be seen that the flow velocity in the lower part is the highest, and the spiral flow formed strikes the curved wall, but then it collides with the upper water flow, resulting in a decreased velocity near the middle-curved wall. Since section 4 is located at the inlet of the first and second curve and is far away from the propeller, the flow pattern is seen as more stable. The flow's velocity decreases and then increases from top to bottom of the channel.

As can be seen from the first curve's velocity pattern (section 5, Figure 14b), the water, resulting from inertial and centrifugal forces, strikes the wall, and thus, a vortex occurs. The high-speed flow driven by the propeller goes upwards after hitting the diversion wall at the bottom, so the flow velocity in the plane increases from the top to the bottom in Row I. The measuring points in Row II are close to the curved wall, so they are strongly influenced by the forced diversion; therefore, the flow velocity at these points fluctuates. The velocity at measuring points Row III is relatively lower than Row II. Under the strong influence of the curved wall in section 6, the water flow is accelerated by the propeller and then diffuses to the upper part. The velocity distribution is lower in the low part and higher in the top part.

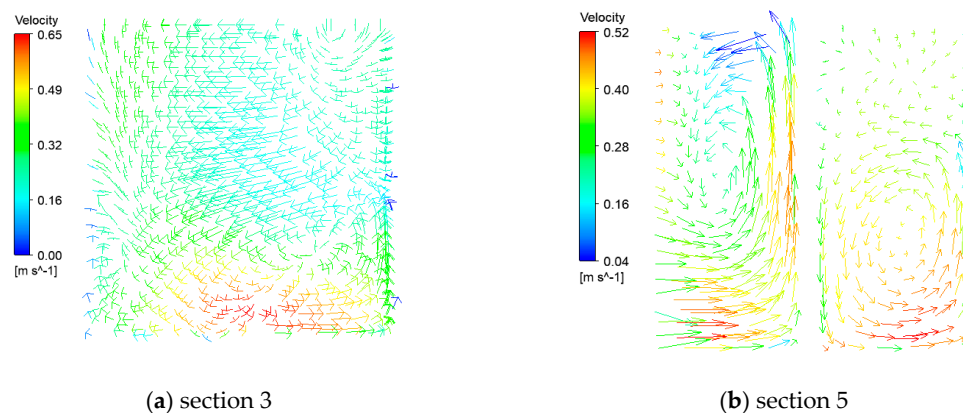


Figure 14. Velocity vectors of different sections.

4. Conclusions

A numerical simulation of water-activated sludge using a two-phase CFD model was used in this paper. The viscosity and settling rate of activated sludge was imported into the FLUENT software through UDF. The influence of the propellers position was analyzed and calculated, and the flow field characteristics of the most appropriate arrangement were compared with the experimental results. The following points can be inferred from results:

(1) In order to meet the energy requirements in the OD, the power of the propeller was selected as 4 kW using the LJM formulation.

(2) When the structure of the oxidation ditch remained unchanged, changing the installation position of the propellers could effectively improve the velocity distribution of OD and reduce sludge deposition. In comparison to the other arrangements, the scheme (b) ($\Delta L = -1L$) provided a more uniform velocity and sludge distribution at the bottom of the oxidation ditch and a lower dead zone

rate. Furthermore, the extreme value of sludge concentration in the whole flow passageway was smaller, so this distribution was the most reasonable propeller configuration.

(3) For each section, a higher velocity did not always result in higher sludge concentration. However, the area with a high dead zone rate usually has a high sludge concentration. As a result, it is reasonable to use a velocity dead zone as a parameter to measure the sludge deposition.

(4) The section of flow velocity obtained by numerical simulation and experiment measurements was similar. Overall, the numerical simulation is able to predict velocities of the measured points in the flow field reasonably well.

Author Contributions: Conceptualization, Y.Z. (Yuquan Zhang), Y.X. and C.L.; investigation, C.L.; writing—original draft preparation, Y.Z. (Yuquan Zhang), H.L., and E.F.-R.; writing—review, Q.T., Y.Z. (Yuan Zheng) and H.L.; writing—editing, Y.Z. (Yuquan Zhang) and Y.X.

Funding: The research was supported by the following funding programs: National Natural Science Foundation of China (51809083); Natural Science Foundation of Jiangsu Province (BK20180504); Fundamental Research Funds for the Central Universities (2019B15114, 2018B48614); China Postdoctoral Science Foundation (2019M651678) and Water Conservancy Science & Technology Project of Jiangsu Province (2018026).

Conflicts of Interest: The authors declare no conflict of interest.

Nomenclature

OD	oxidation ditch	CFD	computational fluid dynamics
UDF	user-defined function	x_i	spatial co-ordinate
p	pressure	ρ	fluid density
μ	dynamic viscosity	\bar{f}_i	time mean external force tensor
$\overline{S_{ij}}$	mean rate of strain tensor	μ_{sv}	sludge viscosity
T	absolute temperature	MLSS	mixed liquor suspended solids
V_s	sludge sedimentation rate	x	sludge concentration
H_f	requirement for pushing 1-kg liquid	$\Sigma\xi$	the overall local resistance factor
F	discharge area	L	length of the OD
U_w	wetted perimeter	U	flow velocity
W_r	power losses for pushing 1-kg liquid	Q_p	discharge through the water section of the OD
W_R	net power for pushing 1-kg liquid	η	efficiency of the propeller

References

1. Yang, Y.; Yang, J.; Zuo, J.; Li, Y.; He, S.; Yang, X.; Zhang, K. Study on two operating conditions of a full-scale oxidation ditch for optimization of energy consumption and effluent quality by using CFD model. *Water Res.* **2011**, *45*, 3439–3452. [[CrossRef](#)]
2. Xie, H.; Yang, J.; Hu, Y.; Zhang, H.; Yang, Y.; Zhang, K.; Zhu, X.; Li, Y.; Yang, C. Simulation of flow field and sludge settling in a full-scale oxidation ditch by using a two-phase flow CFD model. *Chem. Eng. Sci.* **2014**, *109*, 296–305. [[CrossRef](#)]
3. Zhang, Y.; Zheng, Y.; Fernandez-Rodriguez, E.; Yang, C.; Zhu, Y.; Liu, H.; Jiang, H. Optimization design of submerged propeller in oxidation ditch by computational fluid dynamics and comparison with experiments. *Water Sci. Technol.* **2016**, *74*, 681–690. [[CrossRef](#)]
4. Climent, J.; Martínez-Cuenca, R.; Carratalà, P.; González-Ortega, M.; Abellán, M.; Monrós, G.; Chiva, S. A comprehensive hydrodynamic analysis of a full-scale oxidation ditch using Population Balance Modelling in CFD simulation. *Chem. Eng. J.* **2019**, *374*, 760–775. [[CrossRef](#)]
5. Zhou, N.; Dang, C.; Zhao, Z.; He, S.; Zheng, M.; Liu, W.; Wang, X. Role of sludge retention time in mitigation of nitrous oxide emission from a pilot-scale oxidation ditch. *Bioresour. Technol.* **2019**, *292*, 121961. [[CrossRef](#)]
6. Zhang, M.; Yao, J.; Wang, X.; Hong, Y.; Chen, Y. The microbial community in filamentous bulking sludge with the ultra-low sludge loading and long sludge retention time in oxidation ditch. *Sci. Rep.* **2019**, *9*, 1–10. [[CrossRef](#)]
7. Li, X.; Zhang, J.; Zhang, X.; Li, J.; Liu, F.; Chen, Y. Start-up and Nitrogen Removal Performance of CANON and SNAD Processes in a Pilot-scale Oxidation Ditch Reactor. *Process Biochem.* **2019**, *84*, 134–142. [[CrossRef](#)]

8. Liu, Y.; Li, D.; Wei, W.; Lv, B.; Wei, J. Dimensional analysis and numerical simulation methods for the influence of impellers on the average velocity of flows in an oxidation ditch. *Desalin. Water Treat.* **2017**, *81*, 26–32. [[CrossRef](#)]
9. Zhang, Y.; Zhang, J.; Zheng, Y.; Yang, C.; Zang, W.; Fernandez-Rodriguez, E. Experimental Analysis and Evaluation of the Numerical Prediction of Wake Characteristics of Tidal Stream Turbine. *Energies* **2017**, *10*, 2057. [[CrossRef](#)]
10. Behin, J.; Bahrami, S. Modeling an industrial dissolved air flotation tank used for separating oil from wastewater. *Chem. Eng. Process* **2012**, *59*, 1–8. [[CrossRef](#)]
11. Lin, X.; Zhang, J.; Zhang, Y.; Zhang, J.; Liu, S. Comparison of Actuator Line Method and Full Rotor Geometry Simulations of the Wake Field of a Tidal Stream Turbine. *Water* **2019**, *11*, 560. [[CrossRef](#)]
12. Zhang, C.; Zhang, Q.; Zheng, J.; Demirbilek, Z. Parameterization of nearshore wave front slope. *Coast. Eng.* **2017**, *127*, 80–87. [[CrossRef](#)]
13. Luo, L.; Wang, T. Numerical simulation of a combined oxidation ditch flow using 3D k- ϵ turbulence model. *J. Environ. Sci.* **2005**, *17*, 808–812.
14. Yang, Y.; Wu, Y.; Yang, X.; Zhang, K.; Yang, J. Flow field prediction in full-scale Carrousel oxidation ditch by using computational fluid dynamics. *Water Sci. Technol.* **2010**, *62*, 256–265. [[CrossRef](#)] [[PubMed](#)]
15. Wu, S.; Zhou, D.; Zheng, Y. Energy configuration optimization of submerged propeller in oxidation ditch based on CFD. *IOP Conf. Ser. Earth Environ. Sci.* **2012**, *15*, 072012. [[CrossRef](#)]
16. Hartley, K. Controlling sludge settleability in the oxidation ditch process. *Water Res.* **2008**, *42*, 1459–1466. [[CrossRef](#)]
17. Gancarski, P. CFD Modelling of an Oxidation Ditch. Ph.D. Thesis, Cranfield University, Swindon, UK, 2007.
18. Brannock, M. Computational Fluid Dynamics Tools for the Design of Mixed Anoxic Wastewater Treatment Vessels. Ph.D. Thesis, The University of Queensland, Brisbane, Australia, 2003.
19. Gunjal, P.; Ranade, V.; Chaudhari, R. Computational study of a single-phase flow in packed beds of spheres. *AIChE J.* **2005**, *51*, 365–378. [[CrossRef](#)]
20. Aubin, J.; Fletcher, D.; Xuereb, C. Modeling turbulent flow in stirred tanks with CFD: The influence of the modeling approach, turbulence model and numerical scheme. *Exp. Therm. Fluid Sci.* **2004**, *28*, 431–445. [[CrossRef](#)]
21. Wei, J.; Xu, Z. CFD method for the relationship between the radius size of impellers and cross-sectional average velocity of flow in an oxidation ditch. *Desalin. Water Treat.* **2018**, *126*, 127–134. [[CrossRef](#)]
22. Firouz, H.; Sarrafzadeh, M.; Zarghami, R. Modelling a multiple reference frame approach in an oxidation ditch of activated sludge wastewater treatment. In *Frontiers International Conference on Wastewater Treatment and Modelling*; Springer: Cham, Switzerland, 2017; pp. 713–717.
23. Chen, Y.; Ye, L.; Zhao, F. Bacterial Community Shift during the Startup of a Full-Scale Oxidation Ditch Treating Sewage. *J. Microbiol. Biotechnol.* **2017**, *27*, 141–148. [[CrossRef](#)]
24. Fan, L.; Xu, N.; Wang, Z.; Shi, H. PDA experiments and CFD simulation of a lab-scale oxidation ditch with surface aerators. *Chem. Eng. Res. Des.* **2010**, *88*, 23–33. [[CrossRef](#)]
25. Zang, W.; Zheng, Y.; Zhang, Y.; Zhang, J.; Fernandez-Rodriguez, E. Experiments on the mean and integral characteristics of tidal turbine wake in the linear waves propagating with the current. *Ocean Eng.* **2019**, *173*, 1–11. [[CrossRef](#)]
26. Xue, M.; Lin, P. Numerical study of ring baffle effects on reducing violent liquid sloshing. *Comput. Fluids* **2011**, *52*, 116–129. [[CrossRef](#)]
27. Zhang, Y.; Zheng, Y.; Yang, C.; Zhu, Y.; Zhang, X. System design and optimization study of axial flow turbine applied in an overtopping wave energy convertor. *Sadhana* **2015**, *40*, 2313–2331. [[CrossRef](#)]
28. Xue, M.; Chen, Y.; Zheng, J.; Qian, L.; Yuan, X. Fluid dynamics analysis of sloshing pressure distribution in storage vessels of different shapes. *Ocean Eng.* **2019**, *192*, 106582. [[CrossRef](#)]
29. Sánchez, F.; Rey, H.; Viedma, A.; Nicolás-Pérez, F.; Kaiser, A.; Martínez, M. CFD simulation of fluid dynamic and biokinetic processes within activated sludge reactors under intermittent aeration regime. *Water Res.* **2018**, *139*, 47–57. [[CrossRef](#)]
30. Leighton, D.; Acrivos, A. The shear-induced migration of particles in concentrated suspensions. *J. Fluid Mech.* **1987**, *181*, 415–439. [[CrossRef](#)]
31. Zhang, P.; Wu, Z.; Ao, H. Experimental deduction of the relationship between sludge viscosity, concentration and temperature. *Chin. J. Environ. Eng.* **2006**, *7*, 72–74.

32. Rongsen, D. *Theory and Technology of Sewage Treatment in Oxidation Ditch*; Chemical Industry Press: Beijing, China, 2006.
33. Zhang, Y.; Ji, L.; Zheng, Y.; Liu, H.; Xu, X. Nanopatterned metal–organic framework electrodes with improved capacitive deionization properties for highly efficient water desalination. *Sep. Purif. Technol.* **2020**, *234*, 116124. [[CrossRef](#)]
34. Zhang, Y.; Hong, S.; Lin, J.; Zheng, Y. Influence of Ultrasonic Excitation Sealing on the Corrosion Resistance of HVOF-Sprayed Nanostructured WC-CoCr Coatings under Different Corrosive Environments. *Coatings* **2019**, *9*, 724. [[CrossRef](#)]



© 2019 by the authors. Licensee MDPI, Basel, Switzerland. This article is an open access article distributed under the terms and conditions of the Creative Commons Attribution (CC BY) license (<http://creativecommons.org/licenses/by/4.0/>).